Human Molecular Genetics, 2015, Vol. 24, No. 4 **987–993**
doi:10.1093/hmg/ddu513
Advance Access published on October 8, 2014

CACNA1B mutation is linked to unique myoclonus-dystonia syndrome

Justus L. Groen[1,2,5,†], Arturo Andrade[6,†], Katja Ritz[2], Hamid Jalalzadeh[1,2], Martin Haagmans[2], Ted E.J. Bradley[2], Aldo Jongejan[3], Dineke S. Verbeek[7], Peter Nürnberg[9], Sylvia Denome[6], Raoul C.M. Hennekam[4], Diane Lipscombe[6,‡], Frank Baas[1,‡] and Marina A.J. Tijssen[8,‡,*]

[1]Department of Neurology, [2]Department of Genome Analysis and [3]Bioinformatics Laboratory, Clinical Epidemiology, Biostatistics and Bioinformatics and, [4]Department of Pediatrics, Academic Medical Center, University of Amsterdam, Amsterdam, The Netherlands, [5]Department of Neurosurgery, Leiden University Medical Center, Leiden, The Netherlands, [6]Department of Neuroscience, Brown University, Providence RI 02912, USA, [7]Department of Genetics, University of Groningen and [8]Department of Neurology, University of Groningen, Groningen, The Netherlands and [9]Cologne Center for Genomics, University of Cologne, Cologne, Germany

Received April 8, 2014; Revised May 25, 2014; Accepted June 10, 2014

Using exome sequencing and linkage analysis in a three-generation family with a unique dominant myoclonus-dystonia-like syndrome with cardiac arrhythmias, we identified a mutation in the CACNA1B gene, coding for neuronal voltage-gated calcium channels $Ca_V2.2$. This mutation (c.4166G>A;p.Arg1389His) is a disruptive missense mutation in the outer region of the ion pore. The functional consequences of the identified mutation were studied using whole-cell and single-channel patch recordings. High-resolution analyses at the single-channel level showed that, when open, R1389H $Ca_V2.2$ channels carried less current compared with WT channels. Other biophysical channel properties were unaltered in R1389H channels including ion selectivity, voltage-dependent activation or voltage-dependent inactivation. $Ca_V2.2$ channels regulate transmitter release at inhibitory and excitatory synapses. Functional changes could be consistent with a gain-of-function causing the observed hyperexcitability characteristic of this unique myoclonus-dystonia-like syndrome associated with cardiac arrhythmias.

INTRODUCTION

Myoclonus-dystonia syndrome (M-D, MIM #159900) is a rare hyperkinetic movement disorder with myoclonic symptoms (sudden, shock-like movements) combined with dystonia, mainly of the upper part of the body (1). Psychiatric comorbidity has been described, and symptoms often respond to alcohol ingestion (2–4). Up to 50% of individuals with definite M-D have mutations in the *epsilon-sarcoglycan* gene (*SGCE*, DYT11, MIM159900) (5–7). Previously, we described a *SGCE*-negative three-generation pedigree with a unique familial M-D syndrome of unknown cause (8). Affected members of this family ($n = 5$) suffered from cervical and axial dystonia at rest, writer's cramp and action-induced foot dystonia. Myoclonic jerks with on EMG semirhythmic bursts of 40–200 ms occurred in legs and arms during rest. Additional symptoms, not previously described in M-D, include high-frequency continuous myoclonus in the legs while standing causing unsteadiness. Intermuscular and corticomuscular coherences of ~12 Hz were present, and the phase differences suggested an afferent (sensory) cortical input. Eye movement recordings suggest cerebellar pathology. Also present and not previously linked to M-D were cardiac arrhythmias and attacks of painful cramps in upper and lower limbs in three of five affected family members. By combining exome sequencing with linkage mapping in this pedigree, we identified three mutations but focused on a mutation R1389H (rs184841813) in the *CACNA1B* gene that codes for a presynaptic neuronal voltage-gated calcium channels $Ca_V2.2$

*To whom correspondence should be addressed at: Movement Disorders, Department of Neurology, AB 51, University Medical Centre Groningen, PO Box 30.001, 9700 RB Groningen, The Netherlands. Tel: +31 50 3612400; Fax: +31 50 3611707; Email: m.a.j.de.koning-tijssen@umcg.nl
†J.L.G. and A.A. contributed equally to this study.
‡D.L., F.B. and M.A.J.T. contributed equally to this study.

(MIM 601012). By studying single-channel currents of mutant and wild-type human $Ca_V2.2$ channels in a mammalian cell line, we reveal that the R1389H mutation affects the rate of ion flow through single ion channels. These functional analyses of cloned $Ca_V2.2$ channels are consistent with a gain-of-function phenotype.

RESULTS

Patients

We used a 3-generation pedigree for our studies, including 5 of 16 family members suffering from an M-D-plus syndrome previously described (8). (Fig. 1) Features compatible with the known M-D phenotype were cervical and axial dystonia at rest, writer's cramp and action-induced foot dystonia with walking, myoclonic jerks in legs and arms, increasing with action, a positive effect of alcohol on the jerks, and complaints of hyperventilation or panic attacks. However, new prominent features in this pedigree are the high-frequency continuous myoclonus in the legs while standing, causing unsteadiness. Also in three of five affected family members, cardiac arrhythmias and attacks of painful cramps in upper and lower limbs were present (8). Recently, the single brother (III-4) presented with a sudden onset, fixed dystonic posture of the left ankle and wrist, consistent with functional dystonia. No myoclonic jerks or orthostatic myoclonus were noticed. His diagnosis was confirmed by an independent neurologist. This individual was therefore considered unaffected in further study.

CACNA1B R1389H

Linkage analysis assuming a dominant mode of inheritance identified a region of interest of ~150 MB. In this region, five rare heterozygous missense SNVs were found by exome sequencing in affected family member III-2, confirmed by Sanger sequencing. Segregation with disease within the family was seen for three rare SNVs: *CACNA1B* c.4166G>A:p.R1389H, rs184841813 (NM_000718), *VPS13D* c.10355A>G:p.Q3452R (NM_015378) and *SPTAN1* c.5308C>T:p.R1770C, rs371055930 (NM_001130438). These SNVs were not present in 760 (1012 for *CACNA1B*) healthy Dutch controls from the Dutch Blood Bank. Both the *CACNA1B* and *SPTAN1* SNVs are present at very low frequencies in the ±6500 exome variant server (EVS, http://eversusgs.washington.edu/EVS/) (EVS MAF 9.2×10^{-4} and 7.6×10^{-5}, respectively). As M-D is a relatively frequent disorder and EVS participants were not screened for movement disorders, the presence of these variants in EVS is not an argument against their pathogenicity.

The VPS13D Q3452R substitution is predicted to be tolerated (SIFT, PolyPhen) as the amino acid is moderately conserved and there is only a small physiochemical difference between Gln and Arg. The R1770C variant in SPTAN1 and R1389H in CACNA1B are predicted to be deleterious, and residues are well conserved among species. The lack of an association of previously found mutations in *SPTAN1* to M-D leads us to focus on the *CACNA1B* variant. The clinical presentation of myoclonic jerks and dystonia in combination with arrhythmias in this family pointed to a possible channelopathy. The *CACNA1B* gene encodes $Ca_V2.2$, the main of pore-forming alpha-1 subunit of the multi-subunit voltage-gated calcium channel complex that underlies N-type currents in neurons. The preferential location of $Ca_V2.2$ is at nerve terminals, and they play a critical role in controlling transmitter release at many synapses (9). Previously identified pathogenic *CACNA1A* mutations in the homologous region of the gene cause familial hemiplegic migraine (FHM) (V1457L, OMIM 601011.0019) (10) and causing episodic ataxia (type 2) (F1406C, OMIM 601011.0022) (11,12). $Ca_V2.2$ null mice have a major locomotion phenotype, showing significantly more activity [our work, unpublished and (13,14)].

The region of *CACNA1B* coding for the IIIS5 through IIIS6 was Sanger-sequenced in 47 patients with an M-D phenotype. All contained wild-type R1389 and no other novel missense SNVs were identified.

Given the location of R1389 in the extracellular ion pore loop of S5–S6 in CaV2.2 (Fig. 3A), we were able to monitor protein function directly.

Functional analyses R1389H $hCa_V2.2$

To assess the functional consequences of the R1389H mutation on the biophysical properties of Ca_V channels, we expressed

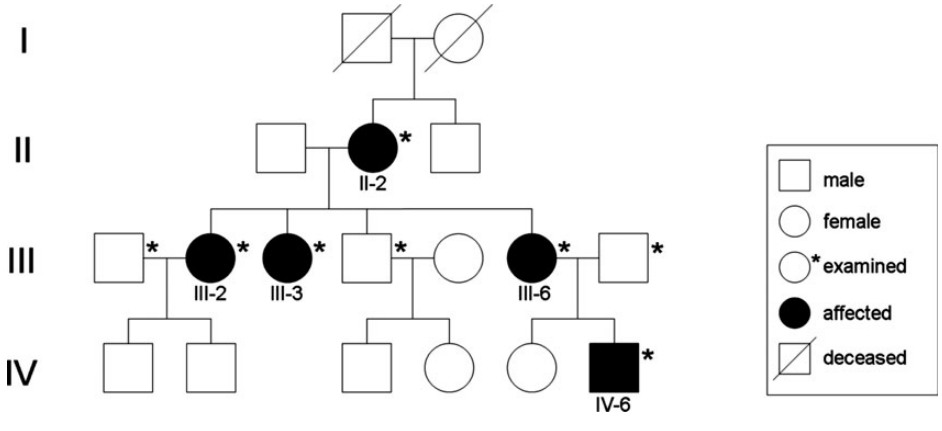

Figure 1. Pedigree of M-D family with R1389H mutation in CACNA1B. Unaffected and affected family members are indicated by clear symbols and blackened symbols, respectively. Diagonal bars through the symbols denote deceased individuals. '*' denotes examined and included in linkage studies. In individual III-2, exome sequencing was performed.

wild-type and mutant hCa$_V$2.2 channels in the mammalian tsA201 cell line and compared calcium channel currents using whole-cell and single-channel patch recordings (Figs. 2–4). Peak and instantaneous current–voltage relationships illustrate that currents through wild-type and R1389H mutant channels reverse direction at close to the same voltages (54 and 52 mV; Fig. 2C and F). This suggests that R1389H has little or no influence on ion selectivity. Channel properties that reflect gating mechanisms such as the voltage dependence of activation and inactivation were also not different between wild-type and R1389H channels (Fig. 2D and E). Thus, the biophysical properties of whole-cell currents were not different, although average whole-cell hCa$_V$2.2 current densities in cells expressing R1389H were larger compared with wild type (Fig. 2A–C). The functional significance of such a difference in current densities in a non-neuronal overexpression system is not clear. The clones are expressed at high level, and several factors contribute to overall current density that are independent of the biophysical properties of the channel but depend on cell-type and subcellular location, including translation efficiency, plasma membrane trafficking and protein stability (17).

We therefore used high-resolution cell-attached patch recordings to make exact measurements of ion flow through single hCa$_V$2.2 wild-type and R1389H mutant ion channels (Figs. 3 and 4). Single-channel currents of R1389H were smaller on average compared with wild type measured under identical conditions (Fig. 3B–D). At +20 mV, the dominant current amplitude of single wild-type channels was 1.03 ± 0.02 ($n = 8$ control patch recordings) compared with 0.77 ± 0.01 for R1389H ($n = 8$ patch recordings; $P = 9.1 \times 10^{-10}$, Student's *t*-test) (Fig. 3B–D). Further analysis revealed that human Ca$_V$2.2 WT channels transition to two different open states the larger of which, O_2 (1.03 pA), dominates and represents ~85% of all openings, compared with O_1 (0.82 ± 0.02 pA, eight patches) (Figs. 3B and 4A). The presence of two different open states in WT recordings is shown as an excess of smaller amplitudes in the amplitude histogram calculated from >500 openings of >0.3-ms duration (Fig. 4A). We observed direct

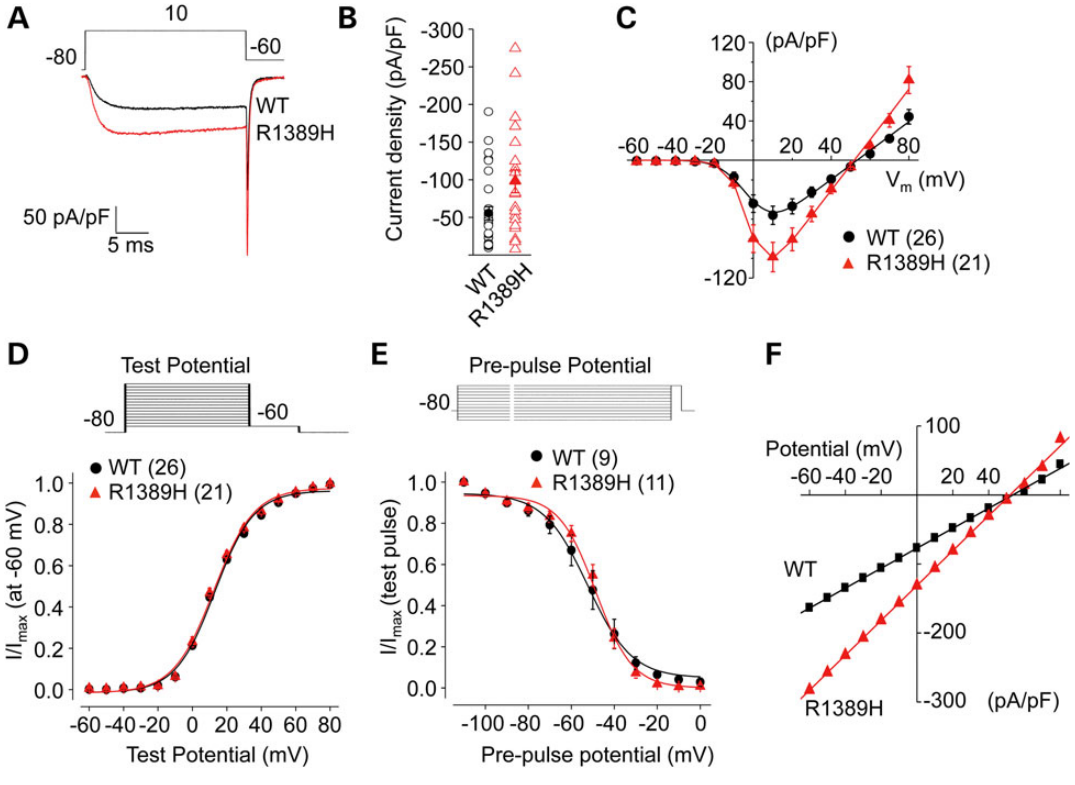

Figure 2. Whole-cell calcium currents recorded from tsA201 cells transiently expressing human R1389H and wild-type control (WT) Ca$_V$2.2 channels. R1389H or WT Ca$_V$2.2 cDNAs were expressed together with Ca$_V\beta_3$ and Ca$_V\alpha_2\delta$-1 and enhanced green fluorescent protein (eGFP). Currents were recorded from fluorescent cells 24 h after transfection using 1 mM calcium as the charge carrier. (**A**) Current traces recorded from cells expressing R1389H or WT Ca$_V$2.2. (**B**) Peak current densities at +10 mV shown together with average values for R1389H: 97.9 ± 15.0 pA/pF (21 cells) and WT: 55.1 ± 9.1 pA/pF (26 cells) ($P = 0.014$, Student's *t*-test). (**C**) Average, peak current–voltage relationships for R1389H and WT. Currents were evoked by depolarizing steps to indicated potentials from a holding potential of −80 mV. Boltzmann-linear functions were fit to individual data sets to estimate average activation mid-point ($V_{1/2}$), slope factor (k) and reversal potential (V_{rev}). Averages ± SE were for R1389H ($n = 21$) and WT ($n = 26$), $V_{1/2}$: −0.18 ± 0.98 and 0.85 ± 1.03 mV ($P = 0.47$); k: 4.8 ± 0.2 and 5.8 ± 0.5 mV ($P = 0.06$) and V_{rev}: 51.6 ± 1.2 and 54.2 ± 0.8 mV ($P = 0.08$). Only currents >40 pA at 10 mV were included in the analysis (~75% of fluorescent cells for R1389H and WT). (**D**) Activation curves measured from tail current amplitudes at −60 mV expressed as I/I_{max} for a range of test potentials. Boltzmann functions were fit to estimate $V_{1/2}$ and k. Average ± SE for R1389H ($n = 21$) and WT ($n = 26$) were for $V_{1/2}$: 12.6 ± 1.1 and 13.6 ± 0.9 mV ($P = 0.47$) and k: 8.4 ± 0.8 and 8.3 ± 0.5 mV ($P = 0.88$). (**E**) Inactivation curves measured as fraction of current available in response to a voltage step to 10 mV from different pre-pulse potentials. Boltzmann functions fit to each data set were used to estimate average ± SE values for R1389H ($n = 11$) and WT ($n = 9$) for $V_{1/2}$: −48.0 ± 1.8 and −51.4 ± 3.8 mV ($P = 0.40$) and k: 10.7 ± 0.3 and 11.6 ± 0.4 mV ($P = 0.09$). (**F**) Instantaneous current–voltage relationship represents the total current flow through all open channels; the data are well fit by a straight line.

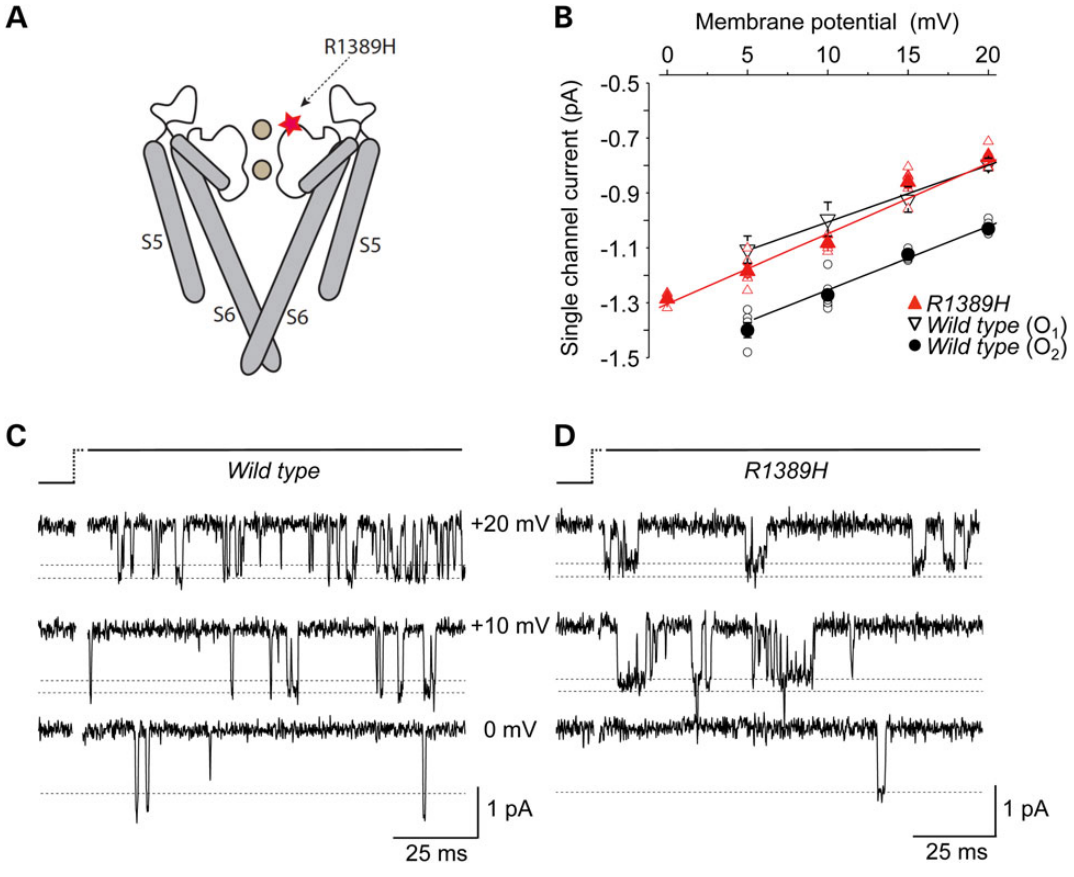

Figure 3. Comparison of current flow through single R1389H and WT control $Ca_V2.2$ channels recorded in cell-attached patches. (**A**) Location of R1389H in the outer region of the $Ca_V2.2$ ion pore (red star) and two calcium ions depicted in the narrow part of the selectivity filter (brown circles) (15,16). (**B**) Single-channel current amplitudes measured from cell-attached patch recordings of R1389H (red triangle) and WT (black circles and open triangles) $Ca_V2.2$ channels. Solid symbols are the average values across patches, and open symbols are averages of 5–100 measurements from channels that were open for long enough to reach full amplitude. WT channels opened to two levels O_1 and O_2, but openings to O_2 dominate (see Fig. 4). Single-channel conductances were between 23 and 27 pS. Examples of recordings of WT (**C**) and R1389H (**D**) channel currents evoked by step depolarizations to +20, +10 and 0 mV. Dotted lines indicate average single-channel current amplitudes at different membrane potentials shown in B.

transitions between O_1 and O_2 within a single opening (Fig. 4B), suggesting that individual $Ca_V2.2$ channels can exist in two open states that conduct ions at different rates. In contrast, single R1389H channels open predominantly to amplitudes that are on average not significantly different from the O_1 amplitude of WT channels (0.77 ± 0.01 pA, $n = 8$ patches; $P = 0.35$, Student's *t*-test) (Fig. 4C and D). Our data suggest that R1389H stabilizes the smaller amplitude open state as compared with WT.

DISCUSSION

We report a missense mutation (c.4166 G>A;p.Arg1389His, rs184841813) in the *CACNA1B* gene in a three-generation family with a myoclonus-dystonia-like syndrome characterized by progressive myoclonic jerks, dystonia and an action-induced lower limb myoclonus combined with cardiac arrhythmias in one pedigree. Clinical and electrophysiological assessment of patients from this family is most consistent with a subcortical origin with possible cerebellar involvement. *CACNA1B* codes for the pore-forming subunit of presynaptic $Ca_V2.2$ channels (MIM 601012) that together with $Ca_V2.1$ (*CACNA1A*) control depolarization-induced calcium entry and transmitter release from the majority of presynaptic terminals at mammalian synapses. Thus, a gain-of-function that influences current flow through the $Ca_V2.2$ channel could directly impact synaptic transmission and could explain the hyperexcitability, characteristic of myoclonus-dystonia syndrome.

After finalizing our studies, the considered unaffected sibling (III-4) presented with a sudden onset, fixed dystonic posture of the left ankle and wrist without myoclonic jerks. His presentation was very different form the affected members and consistent with functional dystonia. We, therefore, still consider him unaffected. His clinical diagnosis was confirmed by an independent neurologist. He did not carry the variant and did not share the same haplotype as affected individuals. This twist in the story illustrates the difficulty of family studies in dystonia.

$Ca_V2.2$ forms a complex with Ca_Va_2d and Ca_Vb subunits that localizes to active zones of presynaptic nerve terminals throughout the brain and nervous system. Together with $Ca_V2.1$, the activity of $Ca_V2.2$ controls the amount of transmitter released in response to depolarization of the presynaptic terminal. At most synapses, the concerted action of $Ca_V2.1$ and $Ca_V2.2$ channels regulates depolarization-dependent presynaptic calcium entry,

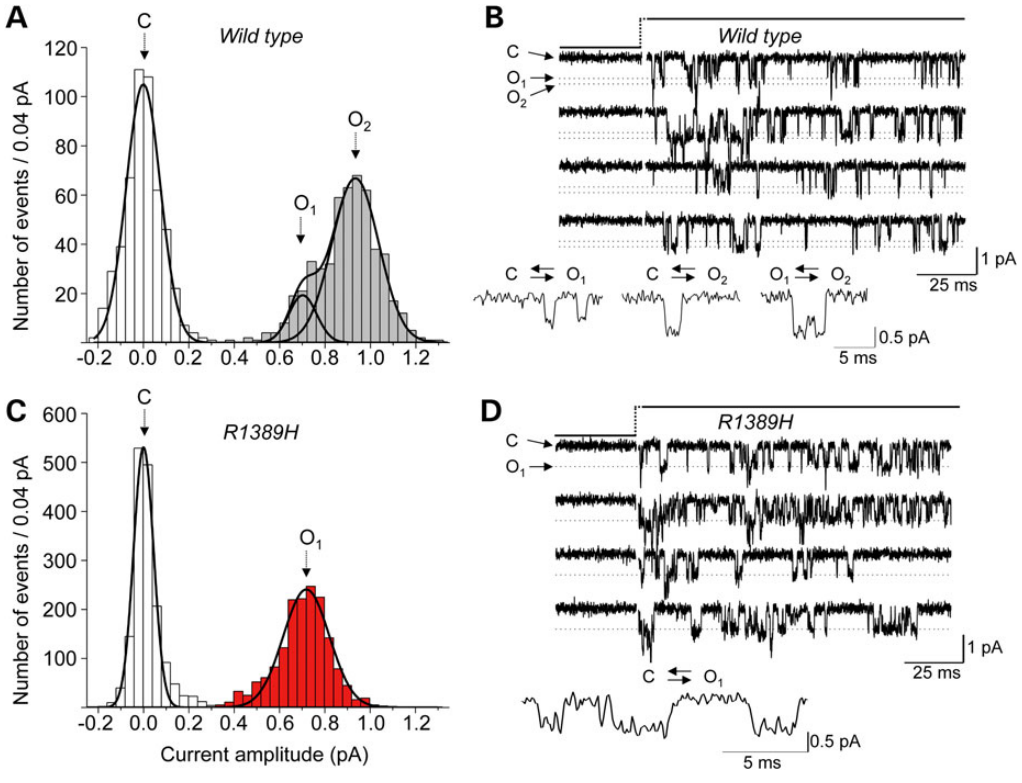

Figure 4. Comparison of single-channel currents in cell-attached patch recordings from WT and R1389H. Amplitude histograms calculated from single-channel analysis of at least 1000 events per cell-attach patch recording of WT (**A**; 1033 events) and R1389H (**C**; 3256 events) channels at +20 mV. Channel open and closed transitions were fit to each event that was longer than 0.3 ms (>3 points). Amplitude histograms of closed (C) and open (O) states were fit with one or the sum of two Gaussian functions. A, O_1: $\mu_? = 0.70$ pA and $A_1 = 2.95$; O_2: $\mu_2 = 0.93$ pA and $A_2 = 17.29$. C,(B) $\mu = 0.67$ pA and $A = 59.5$. Examples of single-channel current are shown for WT (**B**) and R1389H (**D**) channels on two different time-scales. WT $Ca_V2.2$ channels can open from the closed state to two different open levels, O_1 and O_2, and transition directly between O_1 and O_2 without closing. R1389H channels opened to a single level, O_1. Dotted lines indicate average current amplitudes from Gaussian fits (A, C).

whereas at other synapses presynaptic $Ca_V2.1$ or $Ca_V2.2$ channels control calcium entry exclusively (9,18,19). Our functional analyses reveal reduced rate of ion flow through single ion channels compared with wild type. Other essential biophysical channel properties were unaltered in R1389H channels including ion selectivity, voltage-dependent activation or voltage-dependent inactivation. The activation duration of single R1389H mutant channels tended to be longer on average, compared with WT channels. For example, longer activation times of R1389H compared with WT allowed measurements of channel amplitudes at more negative potentials—when channel open times are shorter—and wild-type controls currents were too short to measure accurately (Fig. 3C and D). A longer activation time at the single-channel level could give rise to larger current densities in whole-cell recordings of R1389H compared with wild-type controls (Fig. 2). We did observe consistent differences in the overall expression level of $Ca_V2.2$ channels, but current density measurements depend on several factors that may be influenced by the specific overexpression system used, cell-type, trafficking to and from and stability at the plasma membrane. Thus, the functional significance of this observation remains an open question. In contrast, single-channel current amplitude is an exact measure that is influenced by variables that are readily control in our experiments (concentration of the permeant ion, membrane voltage and temperature.)

Our study is the first to report high-resolution recordings of single human $Ca_V2.2$ channel currents, and they reveal the presence of at least two subconductance states that have important disease relevance. R1389H stabilizes $Ca_V2.2$ channels in the lower current amplitude open state that is observed much less often in wild-type recordings. Subconductance states are a feature of L-type $Ca_V1.2$ channels, and these have been attributed to proton block of ion flow (20–22). Arginine-to-histidine disease-causing mutations occur with relatively high frequency. The R1389H exonic mutation in *CACNA1B* could destabilize potential interactions that depend on the positive charge of arginine at physiological pH such as salt bridge formation between aspartate and glutamate and could result in sensitivity to changes in the extracellular pH. For example, replacement of a highly conserved arginine in the ion pore of an inwardly rectifying potassium channel with histidine reduces the flow of ions through single channels (23).

Mutations in the closely related *CACNA1A* gene are linked to several autosomal dominant neurologic disorders including FHM, episodic ataxia type 2 (EA-2) and spinocerebellar ataxia type 6 (SCA-6). Notably, one of the FHM-causing mutations (V1457L) (10) and a mutation causing EA-2 (F1406C) (11,12) occur in the S5-S6 loop of the *CACNA1A* gene and are in a position homologous to R1389H of CACNA1B. The V1457L $Ca_V2.1$-mutant channel shows lower unitary current

amplitudes compared with wild-type currents, as well as altered channel gating (24).

Surprisingly, mutations in *CACNA1B* have not been demonstrably linked to any human hereditary disorder previously. Common variants in *CACNA1B* are associated with cerebral infarction (25), bipolar disorders and schizophrenia (26,27). Here, we provide evidence that a disruptive missense mutation in the outer region of the ion pore of $Ca_V2.2$ channels may cause a unique M-D syndrome associated with cardiac arrhythmias. Ziconotide (ω-conotoxin MVIIA) is a selective $Ca_V2.2$ channel inhibitor used clinically to relieve otherwise intractable chronic pain and might be a good candidate for therapeutic intervention in our family. By discovering new genes in dominant forms of dystonia, we gain more insight in the pathophysiology of dystonia and hopefully discover promising pharmaceutical therapies for certain forms of (myoclonus) dystonia.

MATERIALS AND METHODS

Patients

All patients were previously described (8). The study was approved by the Medical Ethical Committee of the Academic Medical Center Amsterdam. All patients were examined by a movement disorder specialist (MAJT). Investigations were performed with informed consent.

We performed linkage analysis in this three-generation family and combined these results with the exome data, obtained in the index case.

Linkage analysis

Linkage analysis was performed using the Affymetrix GeneChip Human Mapping 250 K Nsp Array in five affected and one unaffected sibling from three generations. The linkage analysis was performed in family members II-2, III-2, III-3, III-4, III-6 and IV-6 (see Fig. 1). There are four informative meioses in this panel. For a dominant disorder, 0.3 LOD-score points can be obtained per meiosis, providing a maximum LOD score of 1.2. Linkage analysis was performed with the program ALLEGRO making use of a reduced marker panel of ∼20 000 SNPs. Autosomal dominant mode of inheritance with full penetrance was assumed with a disease allele frequency of 0.0001. For the 13 linked regions, again calculations with ALLEGRO were performed with all SNPs from 250K-Chip to determine more accurately the limiting SNPs of the linkage regions.

Exome sequencing

Exome sequencing was performed using enriched libraries (NimbleGen SeqCap EZ Exome v2 Sequence Capture beads) sequenced on a SOLiD v4 platform (Life Technologies), which created paired end reads of 50 bases forward and 35 bases reverse. Color space reads were mapped to the reference human genome (hg18) with SOLiD Bioscope software version 1.3 (Life Technologies). Average coverage of the exome sequencing was 91% for the target, and average depth was 58× after removal of duplicate reads. PCR duplicates were removed prior to variant calling using MarkDuplicates from the Picard software (picard.sourceforge.net/index.shtml). Reads were realigned around known 'indels' with the Genome Analysis Toolkit (Broad Institute). Variants were called using the GATK's Unified Genotyper. GATK's VariantAnnotator was used to annotate variant calls in preparation of filtering. Non-synonymous variants in coding regions that are not present in dbSNP 130 were identified with ANNOVAR (28). SNV population frequency was examined in 760 controls from the Dutch Blood Bank with TaqMan Custom Endpoint Genotyping assays (Applied Biosystems, Foster City, USA). Variants were confirmed by Sanger sequencing.

Electrophysiological analyses of human-derived $Ca_V2.2$ clones

Full-length human $Ca_V2.2$ cDNA (ORF 7094 bp, pSAD442-1) was cloned from human brain and spinal cord and inserted into pcDNA6 mammalian expression vector. pSAD442-1 contains alternate exons (+e10a, +18a, Δ19a, +e31a, +e37b and +e46) (29). The R1389H mutant was generated using standard mutagenesis methods and sequence confirmed. Wild-type and mutant $hCa_V2.2$ were transiently expressed in human tsA201 cells with $Ca_V\beta_3$, $Ca_V\alpha_2\delta$-1 and enhanced green fluorescent protein cDNAs (eGFP; BD Bioscience) as described previously (30). Whole-cell and single calcium channel currents were recorded 24 h after transfection. cDNA concentrations were measured and visualized in agarose gels to ensure these were not different between mutant and wild-type transfections. Recording from wild-type and mutant $Ca_V2.2$ clones were interspersed and the experimenter blind to clone identity during recording and analysis. Macroscopic, whole-cell recordings were obtained from seven separate transfections for both WT and R1389H cDNAs. The identity of WT and that of R1389H clones were revealed post-analysis. Standard whole-cell patch clamp and single-channel recordings were used to compare calcium channel currents (17,30). External solution for whole-cell recordings contained: 1 mM $CaCl_2$, 4 mM $MgCl_2$, 10 mM HEPES, 135 mM tetraethylammonium (TEA) chloride, pH adjusted to 7.2 with TEAOH, and internal solution contained: 126 mM CsCl, 10 mM EGTA, 1 mM EDTA, 10 mM HEPES, 4 mM MgATP, pH 7.2 with CsOH. Whole-cell calcium currents were evoked by voltage-steps and currents leak subtracted on-line using a P/-4 protocol. Data were sampled at 20 kHz and filtered at 2 kHz (−3dB) using an Axopatch 200A amplifier (Molecular Devices, LLC). For single-channel recording, external solution contained: 110 mM $BaCl_2$, 2 mM CsCl, 10 mM HEPES, pH adjusted to 7.2 with BaOH and bath solution contained: 135 mM potassium aspartate, 10 mM EGTA, 5 mM HEPES, 5 mM KCl, pH adjusted to 7.2 with KOH. Electrodes were Sylgard® 184 (Dow Corning, Co) coated and had resistance of 5–8 MW. Single-channel data were sampled at 10–20 kHz and filtered at 2 kHz (−3dB) using Axopatch 200B (Molecular Devices, LLC). Clampfit10 (Molecular Devices, LLC) was used to classify and analyze single-channel events. Leak subtraction was performed off-line by best-fit curve to null traces. All recordings were obtained at room temperature.

ACKNOWLEDGEMENTS

We are grateful to all participants in this study. J.L.G. designed the study and performed genotyping experiments and data

analysis. A.A., S.D. and D.L. cloned the human $Ca_V2.2$ and carried out biophysical analyses. K.R. performed genotype data analysis. H.J. performed genotyping experiments. M.H. performed experiments and data analysis. A.J. assisted with data analysis method development. T.B. assisted in data management and methods development. D.V. and R.C.M.H. assisted with data analysis. P.N. performed linkage analysis. F.B. designed and supervised the study and performed data analysis. M.A.J.T. designed and supervised the study and performed phenotypic analysis. All authors shared in writing the manuscript.

Conflict of Interests statement. None declared.

FUNDING

This work was supported by the Prinses Beatrix Fund (WAR08-06) to M.A.J.T. and K.R. J.L.G. received an AMC Graduate School Scholarship, NIH grants NS055251 to D.L. and 1K99MH099405-01 to A.A.

REFERENCES

1. Klein, C. (2003) Myoclonus and myoclonus-dystonia. Academic Press, Elsevier Science, San Diego, USA
2. Roze, E., Apartis, E., Clot, F., Dorison, N., Thobois, S., Guyant-Marechal, L., Tranchant, C., Damier, P., Doummar, D., Bahi-Buisson, N. *et al.* (2008) Myoclonus-dystonia: clinical and electrophysiologic pattern related to SGCE mutations. *Neurology*, **70**, 1010–1016.
3. Hess, C.W., Raymond, D., Aguiar, P.C., Frucht, S., Shriberg, J., Heiman, G.A., Kurlan, R., Klein, C., Bressman, S.B., Ozelius, L.J. and Saunders-Pullman, R. (2007) Myoclonus-dystonia, obsessive-compulsive disorder, and alcohol dependence in SGCE mutation carriers. *Neurology*, **68**, 522–524.
4. van Tricht, M.J., Dreissen, Y.E., Cath, D., Dijk, J.M., Contarino, M.F., van der Salm, S.M., Foncke, E.M., Groen, J.L., Schmand, B. and Tijssen, M.A. (2012) Cognition and psychopathology in myoclonus-dystonia. *J. Neurol. Neurosurg. Psychiatry*, **83**, 814–820.
5. Ritz, K., Gerrits, M.C., Foncke, E.M., van der Linden, C., Vergouwen, M.D., Bloem, B.R., Vandenberghe, W., Crols, R., Speelman, J.D., Baas, F. and Tijssen, M.A. (2009) Myoclonus-dystonia: clinical and genetic evaluation of a large cohort. *J. Neurol. Neurosurg. Psychiatry*, **80**, 653–658.
6. Zimprich, A., Grabowski, M., Asmus, F., Naumann, M., Berg, D., Bertram, M., Scheidtmann, K., Kern, P., Winkelmann, J., Muller-Myhsok, B. *et al.* (2001) Mutations in the gene encoding epsilon-sarcoglycan cause myoclonus-dystonia syndrome. *Nat. Genet.*, **29**, 66–69.
7. Carecchio, M., Magliozzi, M., Copetti, M., Ferraris, A., Bernardini, L., Bonetti, M., Defazio, G., Edwards, M.J., Torrente, I., Pellegrini, F. *et al.* (2013) Defining the epsilon-sarcoglycan (SGCE) gene phenotypic signature in myoclonus-dystonia: a reappraisal of genetic testing criteria. *Mov. Disord.*, **28**, 787–794.
8. Groen, J., van Rootselaar, A.F., van der Salm, S.M., Bloem, B.R. and Tijssen, M. (2011) A new familial syndrome with dystonia and lower limb action myoclonus. *Mov. Disord.*, **26**, 896–900.
9. Lipscombe, D., Allen, S.E. and Toro, C.P. (2013) Control of neuronal voltage-gated calcium ion channels from RNA to protein. *Trends Neurosci.*, **36**, 598–609.
10. Carrera, P., Piatti, M., Stenirri, S., Grimaldi, L.M., Marchioni, E., Curcio, M., Righetti, P.G., Ferrari, M. and Gelfi, C. (1999) Genetic heterogeneity in Italian families with familial hemiplegic migraine. *Neurology*, **53**, 26–33.
11. Jen, J., Wan, J., Graves, M., Yu, H., Mock, A.F., Coulin, C.J., Kim, G., Yue, Q., Papazian, D.M. and Baloh, R.W. (2001) Loss-of-function EA2 mutations are associated with impaired neuromuscular transmission. *Neurology*, **57**, 1843–1848.
12. Kraus, R.L., Sinnegger, M.J., Koschak, A., Glossmann, H., Stenirri, S., Carrera, P. and Striessnig, J. (2000) Three new familial hemiplegic migraine mutants affect P/Q-type Ca(2+) channel kinetics. *J. Biol. Chem.*, **275**, 9239–9243.
13. Beuckmann, C.T., Sinton, C.M., Miyamoto, N., Ino, M. and Yanagisawa, M. (2003) N-type calcium channel alpha1B subunit (Cav2.2) knock-out mice display hyperactivity and vigilance state differences. *J. Neurosci.*, **23**, 6793–6797.
14. Saegusa, H., Kurihara, T., Zong, S., Kazuno, A., Matsuda, Y., Nonaka, T., Han, W., Toriyama, H. and Tanabe, T. (2001) Suppression of inflammatory and neuropathic pain symptoms in mice lacking the N-type Ca2+ channel. *EMBO J.*, **20**, 2349–2356.
15. Doyle, D.A., Morais, C.J., Pfuetzner, R.A., Kuo, A., Gulbis, J.M., Cohen, S.L., Chait, B.T. and MacKinnon, R. (1998) The structure of the potassium channel: molecular basis of K+ conduction and selectivity. *Science*, **280**, 69–77.
16. Payandeh, J., Scheuer, T., Zheng, N. and Catterall, W.A. (2011) The crystal structure of a voltage-gated sodium channel. *Nature*, **475**, 353–358.
17. Castiglioni, A.J., Raingo, J. and Lipscombe, D. (2006) Alternative splicing in the C-terminus of CaV2.2 controls expression and gating of N-type calcium channels. *J. Physiol.*, **576**, 119–134.
18. Mochida, S., Westenbroek, R.E., Yokoyama, C.T., Zhong, H., Myers, S.J., Scheuer, T., Itoh, K. and Catterall, W.A. (2003) Requirement for the synaptic protein interaction site for reconstitution of synaptic transmission by P/Q-type calcium channels. *Proc. Natl. Acad. Sci. USA*, **100**, 2819–2824.
19. Poncer, J.C., McKinney, R.A., Gahwiler, B.H. and Thompson, S.M. (1997) Either N- or P-type calcium channels mediate GABA release at distinct hippocampal inhibitory synapses. *Neuron*, **18**, 463–472.
20. Hess, P., Prod'hom, B. and Pietrobon, D. (1989) Mechanisms of interaction of permeant ions and protons with dihydropyridine-sensitive calcium channels. *Ann. NY Acad. Sci.*, **560**, 80–93.
21. Pietrobon, D., Prod'hom, B. and Hess, P. (1988) Conformational changes associated with ion permeation in L-type calcium channels. *Nature*, **333**, 373–376.
22. Pietrobon, D., Prod'hom, B. and Hess, P. (1989) Interactions of protons with single open L-type calcium channels. pH dependence of proton-induced current fluctuations with Cs+, K+, and Na+ as permeant ions. *J. Gen. Physiol.*, **94**, 1–21.
23. Yang, J., Yu, M., Jan, Y.N. and Jan, L.Y. (1997) Stabilization of ion selectivity filter by pore loop ion pairs in an inwardly rectifying potassium channel. *Proc. Natl Acad. Sci. USA*, **94**, 1568–1572.
24. Tottene, A., Fellin, T., Pagnutti, S., Luvisetto, S., Striessnig, J., Fletcher, C. and Pietrobon, D. (2002) Familial hemiplegic migraine mutations increase Ca(2+) influx through single human CaV2.1 channels and decrease maximal CaV2.1 current density in neurons. *Proc. Natl Acad. Sci. USA*, **99**, 13284–13289.
25. Yamaguchi, M., Nakayama, T., Fu, Z., Sato, N., Soma, M., Morita, A., Hinohara, S., Doba, N. and Mizutani, T. (2010) The haplotype of the CACNA1B gene associated with cerebral infarction in a Japanese population. *Hereditas*, **147**, 313–319.
26. Curtis, D., Vine, A.E., McQuillin, A., Bass, N.J., Pereira, A., Kandaswamy, R., Lawrence, J., Anjorin, A., Choudhury, K., Datta, S.R. *et al.* (2011) Case-case genome-wide association analysis shows markers differentially associated with schizophrenia and bipolar disorder and implicates calcium channel genes. *Psychiatr. Genet.*, **21**, 1–4.
27. Glessner, J.T., Reilly, M.P., Kim, C.E., Takahashi, N., Albano, A., Hou, C., Bradfield, J.P., Zhang, H., Sleiman, P.M., Flory, J.H. *et al.* (2010) Strong synaptic transmission impact by copy number variations in schizophrenia. *Proc. Natl Acad. Sci. USA*, **107**, 10584–10589.
28. Wang, K., Li, M. and Hakonarson, H. (2010) ANNOVAR: functional annotation of genetic variants from high-throughput sequencing data. *Nucl. Acids Res.*, **38**, e164.
29. Lipscombe, D., Andrade, A. and Allen, S.E. (2013) Alternative splicing: functional diversity among voltage-gated calcium channels and behavioral consequences. *Biochim. Biophys. Acta*, **1828**, 1522–1529.
30. Raingo, J., Castiglioni, A.J. and Lipscombe, D. (2007) Alternative splicing controls G protein-dependent inhibition of N-type calcium channels in nociceptors. *Nat. Neurosci.*, **10**, 285–292.